Graphical Abstract

Economics of an Additive Manufactured Heat Exchanger for Concentrating Solar Power

Tracey Ziev, Erfan Rasouli, Ines-Noelly Tano, Ziheng Wu, Srujana Rao Yarasi, Nicholas Lamprinakos, Vinod Narayanan, Anthony D. Rollett, Parth Vaishnav

Highlights

Economics of an Additive Manufactured Heat Exchanger for Concentrating Solar Power

Tracey Ziev, Erfan Rasouli, Ines-Noelly Tano, Ziheng Wu, Srujana Rao Yarasi, Nicholas Lamprinakos, Vinod Narayanan, Anthony D. Rollett, Parth Vaishnav

- Integrating cost modeling with heat exchanger design processes can identify avenues to reduce costs without compromising heat exchanger thermo-mechanical performance.

- Transitioning to industrial scale AM technologies can reduce costs. Additional industrial application-oriented AM innovations can further reduce costs.

Economics of an Additive Manufactured Heat Exchanger for Concentrating Solar Power

Tracey Ziev[a], Erfan Rasouli[b], Ines-Noelly Tano[b], Ziheng Wu[c], Srujana Rao Yarasi[c], Nicholas Lamprinakos[c], Vinod Narayanan[b], Anthony D. Rollett[c], Parth Vaishnav[d,a]

[a]*Department of Engineering and Public Policy, Carnegie Mellon University, 5000 Forbes Avenue, Pittsburgh, 15213, PA, USA*
[b]*Department of Mechanical and Aerospace Engineering, University of California, Davis, One Shields Avenue, Davis, 95616, CA, USA*
[c]*Department of Materials Science and Engineering, Carnegie Mellon University, 5000 Forbes Avenue, Pittsburgh, 15213, PA, USA*
[d]*School for Environment and Sustainability, University of Michigan, 440 Church Street, Ann Arbor, 48109, MI, USA*

Abstract

Developing low cost, high efficiency heat exchangers (HX) for application in concentrated solar power (CSP) is critical to reducing CSP costs. However, the extreme operating conditions in CSP systems present a challenge for typical high efficiency HX manufacturing processes. We describe a process-based cost model (PBCM) to estimate the cost of fabricating an HX for this application using additive manufacturing (AM). The PBCM is designed to assess the effectiveness of different designs, processes choices, and manufacturing innovations to reduce HX cost. We describe HX design and AM process modifications that reduce HX cost from a baseline of \$780/kW-th to \$570/kW-th. We further evaluate the impact of alternative current and potential future technologies on HX cost, and identify a pathway to further reduce HX cost to \$270/kW-th.

Keywords: Manufacturing cost, Additive manufacturing, Pin fin heat exchanger, Concentrating Solar Power, Techno-economic modeling

1. Introduction

In 2011, the U.S. Department of Energy (DOE) launched the SunShot 2020 initiative to improve the cost-competitiveness of large scale solar power

by reducing its cost up to 75% from 2010 cost [1]. By 2017, the U.S. solar industry had made substantial progress towards achieving SunShot 2020 goals. The DOE identifies Concentrating Solar Power (CSP) with thermal energy storage as a technology that inherently addresses grid integration challenges due to its storage capacity. As such, SunShot 2030 added goals specific to CSP with thermal storage, setting higher levelized cost of electricity (LCOE) targets for CSP compared to solar photovoltaic (PV), in recognition of the value of CSP dispatchability. The SunShot 2030 targets for CSP are to reduce LCOE from $0.10/kWh to $0.05/kWh for baseload plants with at least 12 hours of thermal storage and from $0.18/kWh to $0.10/kWh for peaker plants with less than 6 hours of thermal storage [2].

In its "On the Path to SunShot" series, the DOE identified the demonstration of a high-temperature power cycle, such as the supercritical carbon dioxide (sCO$_2$) Brayton cycle, as a critical development necessary to increase cycle efficiency to achieve CSP SunShot cost targets [3]. The requirements for this system include $\geq 50\%$ thermal-electric cycle efficiency, $\geq 700°$C hot-side temperature, ≥ 20 MPa operating pressure, and a powerblock cost of $\leq \$900/kW_e$ [3]. Currently, heat exchangers (HX) account for 60 - 70% of sCO$_2$ Brayton cycle powerblock cost [4]. To meet the powerblock cost requirement for CSP, substantial cost reductions for the primary HX, which is located at the high temperature and high pressure side of the cycle, are needed. Currently, the baseline technology for fabricating a high efficiency HX is a diffusion bonding based microlamination process. In microlamination, the HX is fabricated by photochemically etching a channel pattern onto thin metal shims, stacking the shims, diffusion bonding under high temperature and pressure, and welding traditionally manufactured inlet and outlet headers to the diffusion bonded core [5]. Investigations of diffusion bonding with high temperature resistant alloys (Haynes 230 and Haynes 282) have shown that defects form in the bond region that reduce the creep and fatigue life of the bonded material as compared to the material's sheet form [6, 7]. In addition to the technical challenge of diffusion bonding high temperature resistant alloys, microlamination produces relatively expensive HX. The "On the Path to SunShot" series identifies a need for alternative HX designs and manufacturing processes to reduce primary HX cost [3].

Additive manufacturing (AM) holds promise as an alternative technique for manufacturing high efficiency HX. AM creates parts directly from a 3D CAD model by slicing the CAD model into thin layers, then adding material layer by layer until the final part is fully formed. This technique enables

manufacturing of complex parts with intricate geometries, including internal passages, that would be difficult or impossible to fabricate via traditional manufacturing processes [8]. This advantage of AM can be leveraged for manufacturing high efficiency, compact HX. AM HX incorporate microscale heat transfer features to increase HX efficiency while maintaining or decreasing HX size [9]. Direct Laser Metal Sintering (DLMS), a form of AM where a laser melts metal powder to form each layer of the part, has been successfully used to demonstrate fabrication of AM HX designs for aerospace and power generation applications [9, 10, 11, 12]. These investigations of using AM for HX design focus primarily on design for HX performance, with limited consideration of manufacturing cost.

We use Process Based Cost Modeling (PBCM) to evaluate the cost of manufacturing an AM HX for use as the molten salt (MS)-to-(sCO$_2$) primary HX for CSP systems. We chose PBCM because it enables us to integrate cost into the part and manufacturing process design process [13]. PBCM builds the total part cost from the costs associated with each step of the manufacturing process. The cost for each process step is modeled from the contributing components of cost (e.g. capital, material, labor, etc.) and their relationship to the part's design (e.g. dimensions, material choice, etc.), processing parameters (e.g. cycle time, heating/cooling time, etc), and facility operating parameters (e.g. operating hours, production volume, etc.) [14]. PBCM has been used to estimate costs for a variety of applications including, automotive [15], aerospace [16], and energy storage [17, 18]. PBCM can also be used in conjunction with other physical and logistical models to simultaneously design for multiple objectives. This approach has been used to co-evaluate cost and supply chains[19], part consolidation [20], and part structure [21]. Cost models for the production of microchannel HX exist [22, 23, 24], but these models are typically developed post-hoc rather than being integrated into the HX and manufacturing process design process. We integrate our PBCM with the HX performance model and use it as a tool to enable an iterative design process for the HX and AM process.

Our PBCM estimates the cost of a four-step AM process consisting of direct laser metal sintering (DLMS) followed by post-processing operations as shown in Figure 1. The first post-processing operation is removing the HX from the support structures and base with a computer numerically controlled (CNC) band saw. The next operation is a heat treatment to relieve residual stresses in the HX. These two post processing operations are the minimum post processing required for any DLMS build. The final post-processing
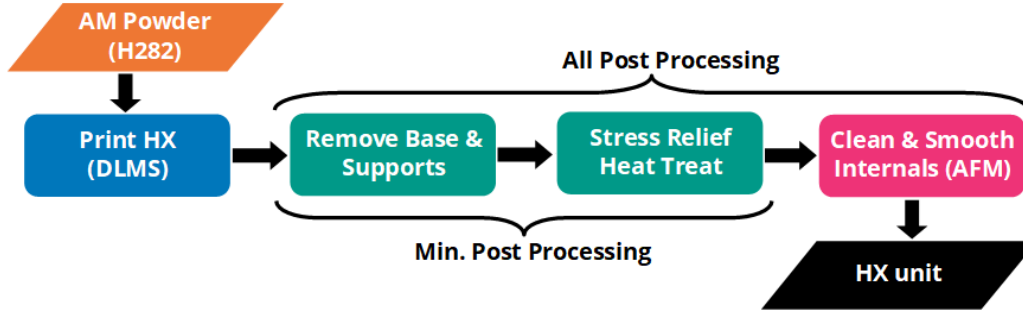
3

Figure 1: Our PBCM models a four-step AM process: HX printing via DLMS, stress relief heat treating, removing supports and base plate, and internal passage cleaning via abrasive flow machining (AFM).

step we model is internal passage cleaning and smoothing via abrasive flow machining (AFM) which forces an abrasive polymer through the part to smooth the surfaces.

2. Heat Exchanger and Manufacturing Process Design

To evaluate the potential for use of an AM heat exchanger for solar thermal applications, we designed a small-scale MS-to-sCO$_2$ heat exchanger, shown in Figure 2, which is described in the rest of this manuscript. The design requirements for the small-scale HX are identical to that for the larger scale, with the exception of the heat transfer rating (in kW-th). The hot side fluid is molten chloride salt (MS) at a nominal pressure of 1 bar that enters at a temperature of 720 °C from a hot storage tank or from the molten salt receiver. The cold side fluid is sCO$_2$ that enters the HX at a temperature of 500 °C. The nominal pressure on the sCO2 side is 200 bar. Haynes 282, a Ni superalloy, is chosen as the material for the HX due to its high creep strength at the design operating temperatures [25]. The HX design consists of a series of spaced plates connected via sCO$_2$ inlet and outlet headers. Molten salt flows around and between the plates. The core of the HX consists of repeating pin array sCO$_2$ channels and finned MS channels. The pin spacing and diameter are determined based on structural integrity considerations. On the sCO2, additional structures are added at the inlet and exit locations to improve flow distribution and maintain structural integrity on the sCO$_2$ side of the HX. We chose straight fins on the MS side to increase heat transfer while minimizing pressure drop and allowing for gravity drainage. The initial

4

dimensions of the plate array portion of the HX are length, l_p, of 240 mm, width, w_p, of 100 mm, and height, h_p, of 50 mm. The baseline dimensions of each of the two header portions of the HX are length, l_h, of 60 mm, width, w_h, of 160 mm, and height, h_h, of 60 mm. Multiple such HX can be combined using common headers to form a multi-MW scale HX for the primary MS-to-sCO$_2$ HX for CSP.

We considered several performance aspects in the design of the HX including sCO$_2$ pressure drop, drainage of MS, thermal and flow characteristics, thermal stresses, creep, and fatigue. We initiated the design process by determining the geometry of a repeating unit cell of the pin array that would be able to withstand the mechanical pressure of 200 bar. We designed the HX to ensure that the HX core did not experience a stress in excess of the design limit of 100 MPa (based on rupture strength of H282 for 100,000 hours of operation). After obtaining the limits of the pin array dimensions that would meet this stress requirement, we developed thermofluidic model to determine the optimal dimensions of the HX in terms of effectiveness and gravimetric and volumetric power density. Once we identified the optimal core geometry, we designed the sCO$_2$ headers for mechanical strength and to ensure uniform flow distribution (see Figure 2). The flow paths within each sCO$_2$ pin array between the headers and the counter-current region (see Figure 2, bottom right detail) also ensure uniform flow across the height of each pin array. We performed a conjugate computational fluid dynamics simulation on a pair of hot and cold channels in the core to determine the thermal stresses in the geometry, including the headers. Following a complete thermo-mechanical design of the HX, we performed creep simulations, based on the Norton model, on the core and header regions to determine whether the HX could operate for 100,000 hours at the design temperature and pressure for both continuous and cyclic operation.

We evaluate production of the small-scale HX design via DLMS in an EOS M290 machine. The EOS M290 has a single 400 W laser with a build area of 250 mm x 250 mm x 375 m [26]. Several key controllable parameters control the DLMS process including laser power, P, laser scan speed, v, hatch spacing (distance between laser scan passes), H, and layer thickness, L. The DLMS processing parameters impact the time required for printing; build rate for the part is approximately proportional to vHL. Increasing v, H, and/or L will increase the build rate which reduces print time and in turn reduces cost. The DLMS processing parameters also impact the defects content of the part, which has been shown to degrade fatigue life
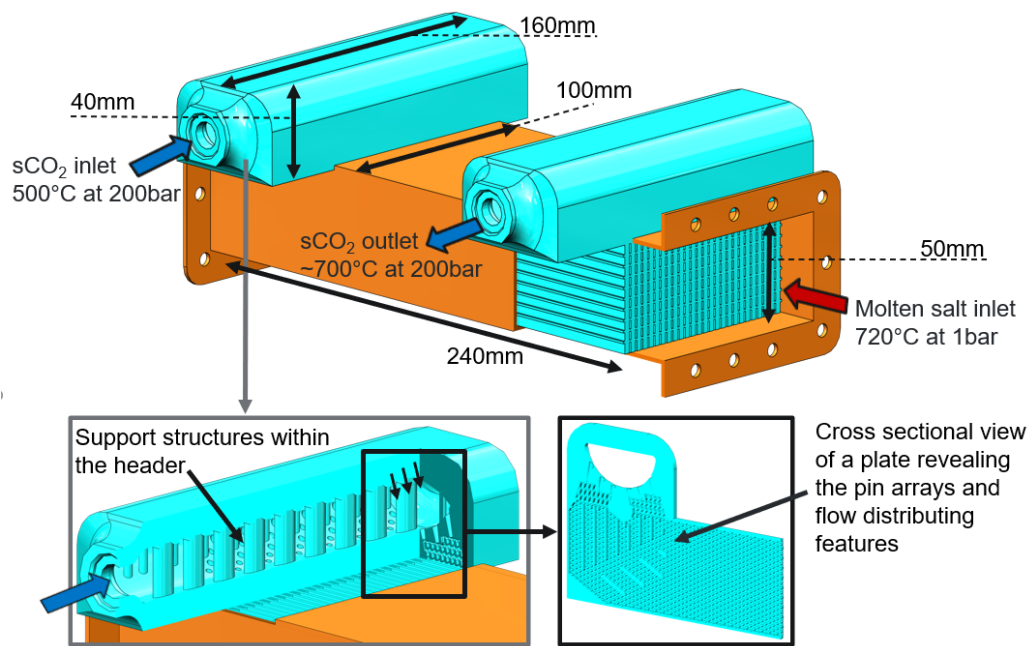
Figure 2: Heat exchanger design shown on EOS M290 build plate (250 mm x 250 mm) with sections showing of header internals and sCO_2 side micropin features.

of AM parts [27, 28]. Porosity defects in DLMS are correlated with energy density, E, which is approximately proportional to $\frac{P}{vHL}$ [29]. At low E, lack of fusion porosity occurs due to incomplete melting of the powder. At high E, keyhole porosity occurs due to instability in the meltpool. At combinations of high P and v, bead-up occurs causing porosity and/or contact with the the powder recoater blade [30, 31, 32]. We can select processing parameters for HX printing from within the region bounded by these three porosity defect regimes. For our baseline cost, we conservatively use process parameters that produced the lowest porosity during parameter set testing in Haynes 230 (a similar material to H282, also evaluated as a potential material for the HX). Our baseline parameter set uses P of 370 W, v of 700 mm/s, H of 110 microns, and L of 40 microns.

3. Methods

3.1. Process Based Cost Modeling

Our PBCM models HX total cost as a sum of the costs for each process step and material cost, c_{mat}, as shown in Equation 1. The cost for each process step is modeled as a function of equipment cost, c_{equip}, labor cost, c_{labor}, facility cost c_{fac}, consumables cost, c_{cons}, utility cost, c_{util}, and overhead cost, c_{over}. As described below and much more extensively in the supplemental materials, we collected input data for the model from multiple sources including existing literature, trade and vendor publications and websites, vendor quotes, and discussions with AM experts. The cost of each step accounts for the yield of previous steps and the material cost accounts for the overall yield of the process as well as the loss of some fraction of the excess metal powder that cannot be recovered and recycled.

$$c_{unit} = c_{mat} + c_{eq} + c_{lab} + c_{fac} + c_{cons} + c_{util} + c_{over} \qquad (1)$$

To account for uncertainty in the cost estimate, We conduct Monte Carlo simulations that randomly vary key input parameters for 3D printing costs. We represent each input parameter as a uniform random distribution; each iteration of the Monte Carlo simulation randomly sampled from each parameter's distribution. For each calculation where uncertainty is represented, we conduct 1,000 iterations of the Monte Carlo simulation, and calculate the mean and standard deviation of the samples. We report 2 standard deviations as the uncertainty range for these costs.

3.1.1. Annual and Effective Production Volumes

In our model, we specify the number of HX to be produced each year, the annual production volume (APV). We use APV 1,500 units for our baseline, the approximate number required for a single 20 MW CSP plant. To account for defective parts, we calculate an effective production volume, EPV, required to produce the APV of saleable units. We calculate EPV as a function of APV and the product of the part acceptance rates, y_{ps} for each of n_{ps} process steps from Figure 1, as shown in Equation 2. We use EPV as the quantity input to calculate total cost for each cost category then divide by APV to distribute cost across the saleable units. We assume y_{ps} 80-95% for HX printing, 100% for stress relief heat treating, 98% for removing supports/base plate, and 99% for cleaning and smoothing internal passages based on input from Carnegie Mellon University (CMU) NextManufacturing and equipment vendors.

$$EPV = \frac{APV}{\prod_{i=1}^{n_{ps}} y_i} \qquad (2)$$

3.1.2. Material Cost

We calculate material cost per unit, c_{mat}, as a function of HX mass (adjusted to account for process yield), m, scrap rate, r_s, and material price, p_{mat}, as shown in Equation 3. For H282, we use a range of \$125-145/kg based on the vendor-quoted price of \$139/kg. We assume r_s to be 5-15% based on the 10% recommendation from CMU NextManufacturing [33].

$$c_{mat} = p_{mat} m (1 + r_s) \qquad (3)$$

3.1.3. Equipment Cost

For each process step, we calculate annual cost of equipment as a function of machine price, p_{mch}, an equipment capital recovery factor, CRF, installation price, p_{inst}, annual maintenance cost, p_{mnt}, and number of machines required to produce EPV units, n_{mch}, as shown in Equation 4.

$$c_{eq} = \frac{n_{mch}(CRF p_{mch} + p_{inst} + p_{maint})}{APV} \qquad (4)$$

We use p_{mch} \$535,000-700,000 for HX printing [34], \$50k for stress relief heat treating [16], \$65k for removing supports/base plate via band saw [35], and \$170k for cleaning and smoothing internal passages via AFM (vendor quote). We calculate CRF as a function of discount rate, d, and expected

machine life, t_{ml}, as shown in Equation 5. We use the average US small business discount rate of 8.5% [36] for d. For t_{ml}, we use the average 3D printer life of 7-10 yrs for HX printing [37], and for all other process steps assume t_{ml} 20 yrs.

$$CRF = \frac{d(1+d)_{ml}^{t}}{(1+d)_{ml}^{t} - 1} \qquad (5)$$

For p_{inst}, we use \$47k for HX printing [34], and for all other process steps assume p_{inst} is 10% of p_{mch}. For c_{mnt}, we use \$58k for HX printing [34], and for all other process steps assume p_{mnt} is 5% of p_{mch} per year. We calculate n_{mch} as a function of EPV, annual machine operating hours, t_{op}, machine set-up/teardown time (including heat-up/cooldown time), t_{st}, and cycle time, t_{cyc}, as shown in Equation 6. We assume t_{op} 8064 hrs (92% up time). We assume t_{st} 9.5 hrs for HX printing, 8hrs for stress relief heat treating, 0.5 hrs for removing supports/base plate, and 0.5 hrs for cleaning and smoothing internal passages based on input from CMU NextManufacturing and equipment vendors. For our baseline case, we used t_{cyc} 135 hrs $+/-10\%$ for HX printing (see Section 3.1.4), 4 hrs for stress relief heat treating, 6 hrs for removing supports/base plate, and 1 hr for cleaning and smoothing internal passages based on input from CMU NextManufacturing and equipment vendors.

$$n_{mch} = \frac{EPV(t_{st} + t_{cyc})}{t_{op}} \qquad (6)$$

3.1.4. HX Print Time

We divide our print time calculation into two parts, raster time, t_r, and powder spread time, t_{ps}. To calculate t_r, we divide the HX into segments that can be approximated as having a constant cross-section. For each segment, we calculate t_r as a function of HX height, h, width, w, and length l, laser scan speed, v, hatch spacing, H, layer thickness L, and end of raster pause time, t_{rp}, as seen in Equation 7. The supplemental materials contain a detailed description of the print time calculation. For our baseline, with use v of 700 mm/s, H of 110 microns, and L of 40 microns. We assume t_{rp} of 3 milliseconds.

$$t_r = \frac{h}{L}\left[\frac{w}{H}\left(\frac{l}{v} + t_{rp}\right) + \frac{2(w+H)}{v} + 3t_{rp}\right] \qquad (7)$$

We calculate powder spread time as a function of h, L, build plate length (250mm [26]), time to raise platform, t_{plat}, recoater spread speed v_{rs}, and recoater return speed v_{rr}. We use t_{plat} 2s, v_{rs} 150 mm/s and v_{rr} 500 mm/s.

$$t_{ps} = \frac{h}{L} \left(\frac{250}{v_{rs}} + \frac{250}{v_{rr}} + t_{plat} \right) \tag{8}$$

3.1.5. Labor Cost

For each process step, we calculate annual labor cost as a function of number of laborers, n_{lab}, annual salary, p_{lab}, and labor burden rate, r_{lab}, as shown in Equation 9.

$$c_{lab} = \frac{n_{lab}p_{lab}(1 + r_{lab})}{APV} \tag{9}$$

For our baseline, we use p_{lab} of \$36,000-88,000 based on salary ranges for an engineering technician [38].For r_{lab}, we use the US average of 30% [39]. We calculate n_{lab} as a function of t_{mch}, labor fraction, f_{lab}, and annual manufacturing labor hours per full time laborer, t_{lab}, as shown in Equation 10. For our baseline, we estimate f_{lab} to be 3-13% for HX printing, 5% for stress relief heat treating, 26% for removing supports/base plate, and 50% for cleaning and smoothing internal passages. These numbers are calculated by estimating the ratio of the process that requires labor to the total duration of the process (see the supplemental materials for setup/teardown, heatup/cooldown, and cycle times and labor fractions). We assume t_{lab} 1632 hrs.

$$n_{lab} = \frac{f_{lab}t_{mch}}{t_{lab}} \tag{10}$$

3.1.6. Facility Cost

For each process step, we calculate annual facility cost as a function of n_{mch}, machine floor space, A_{mch}, machine clearance space, A_{clr}, facility rental price p_{fac}, facility buildout price p_{build}, and CRF as shown in Equation 11. We use A_{mch} 16m² for HX printing [26], 5.4m² for stress relief heat treating [16], 16m² for removing supports/base plate [16], and 8m² for cleaning and smoothing internal passages [40]. We assume a clearance space of 200% A_{mch}. For p_{fac}, we use the US average industrial facility rent price of \$749/m² [41]. For p_{build}, we use \$4,300-5,400/m²/month based on consultation with

CMU NextManufacturing experts. We assume 20 yr amortization periods to calculate CRF for the facility build out.

$$c_{fac} = \frac{n_{mch}(A_{mch} + A_{clr})(p_{fac} + p_{build} * CRF)}{APV} \qquad (11)$$

3.1.7. Consumables Cost

For each process step, we calculate the consumable materials used during the process as a function of consumable price, p_c, rate of consumption, r_c (depending on consumable, either per hour of cycle time or per part), EPV, and t_{cyc} (for consumables with a per hour-based r_c), as shown in Equation 12. For HX printing, we model build plates (p_c \$700/plate [34], r_c 1 plate/10 HX) and filters(p_c \$600/filter set [34], r_c 1 filter set/3600 hrs). For removing supports/baseplate, we model blades (p_c \$190/blade [42], r_c 1 blade/1440 hrs) and cutting fluid (p_c \$8.40/L [43], r_c 60 L/hr[44]). Stress relief heat treating does not require consumables. For internal passage cleaning and smoothing, we model abrasive medium (p_c \$3500/machine fill, r_c 1 machine fill/machine/21,600 hrs (from vendor estimate)). All r_c values are based on estimates from equipment vendors and CMU NextManufacturing.

$$c_{cons} = \frac{\frac{p_c EPV t_{cyc}}{r_c}}{APV} \qquad (12)$$

3.1.8. Utility Cost

We assume that all utilities except electricity are negligible. For each process step, we calculate annual utility cost as a function of t_{mch}, machine electricity use, r_{el}, and electricity price p_{el}. We use r_{el} of 16.7kW for HX printing [26], 6.2kW for stress relief heat treating [16], 7.8kW for removing supports/base plate [16], and 7.5kW for cleaning and smoothing internal passages [40]. For p_{el}, we use the US industrial electricity prices of \$0.067-0.248/kWh[45].

3.1.9. Overhead Cost

Overhead accounts for costs such as management, quality assurance, human resources, environmental health & safety, cleaning, accounting, administrative services, legal services, office space, inventory storage, building utilities (lights, heat, etc.), shipping/packing, office supplies, and IT equipment. We estimate total overhead cost based on typical small business costs for

these goods and services. The supplemental materials contain a detailed description of the overhead calculation. At APV 1,500, overhead costs are equal to approximately 17% of total non-overhead costs. We distribute overhead cost across process steps by allocating a fraction of overhead cost to each step equal to the fraction of total non-overhead cost associated with that step.

4. Results

Figure 3 shows the cost per kW for our baseline HX design as a function of the number of HX units manufactured per year (annual production volume - APV). The cost per kW decreases rapidly with increasing APV, reaching economies of scale at between 50 - 100 units/year. This production quantity is well below the quantity of HXs required for a single 20 MW CSP plant (approximately 1,500 units, 12.7 kW/unit). At an APV of 1,500 units, our initial HX design costs approximately $780/kW-th ($660-780/kW-th). We evaluated breakdowns of the HX cost by process step and cost category to identify opportunities to reduce HX cost.

Figure 4 shows a breakdown of HX cost per kW-th by manufacturing process step at APVs of 10, 20, 50, 100, and 1,500 units. This breakdown shows that the HX AM step is the most significant contributor to HX cost, accounting for approximately 65% of total cost at 1,500 units. Figure 5 shows HX cost per kW-th with AM cost broken down by cost category at APVs of 10, 20, 50, 100, and 1,500 units. At all production volumes, equipment is the most significant contributor to AM cost. AM equipment cost is dependent on the the cycle time (print time) for the AM process. Figure 6 shows HX cost per kW-th with AM cost broken down by cost category for build times of 25, 50, 75, 100, 150, and 200% of the baseline print time (135 hours). This shows that cost in most AM cost categories decreases as build time decreases. We therefore focused our initial efforts to identify cost reduction opportunities on decreasing build time without changing HX performance.

Reducing the amount of material used in the HX, thereby reducing the amount of material that must be melted during printing, will reduce the print time (and also material cost). However, changing the geometry of the pin array section of the HX affects the thermal performance of and pressure drop across the HX. The header geometry is not expected to substantially impact HX thermal performance or pressure drop, provided that the change does not change flow distribution uniformity within the pin array. Reducing header volumes by 25% reduces material use by approximately 12%, print
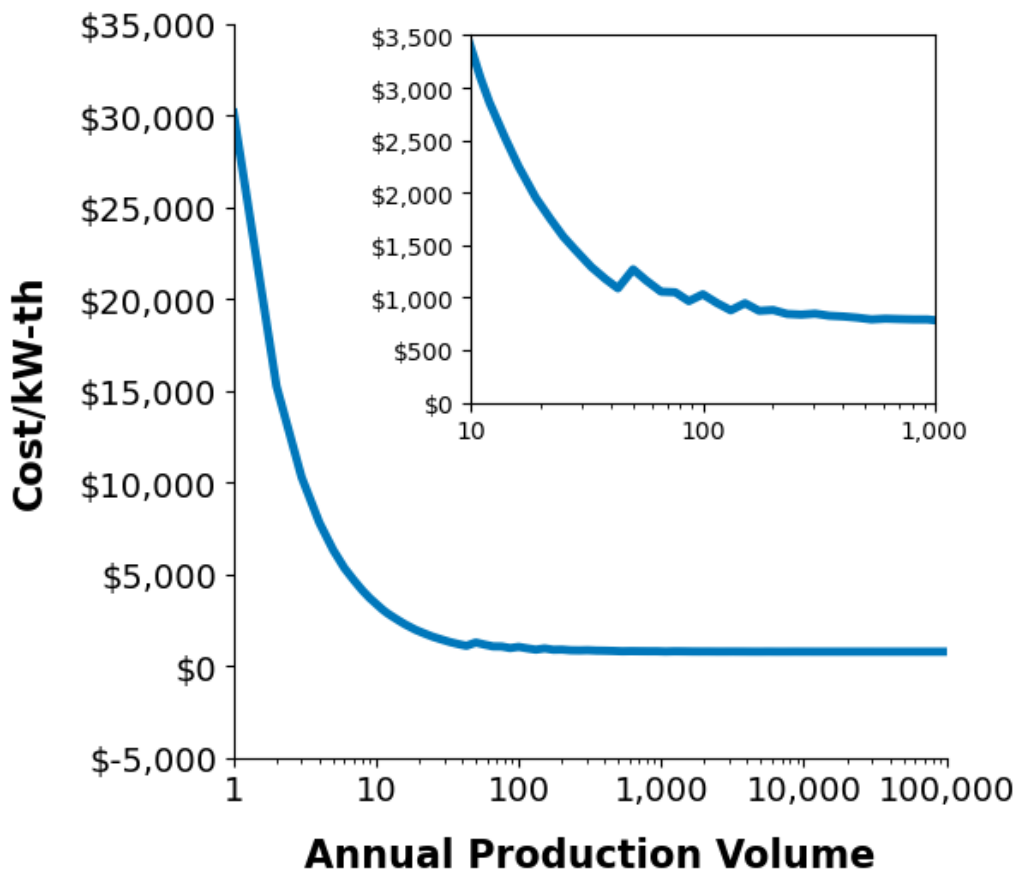
Figure 3: For our initial design, economies of scale are achieved at APV 50-100 units. At APV 1,500, our design costs approximately $780/kW-th.
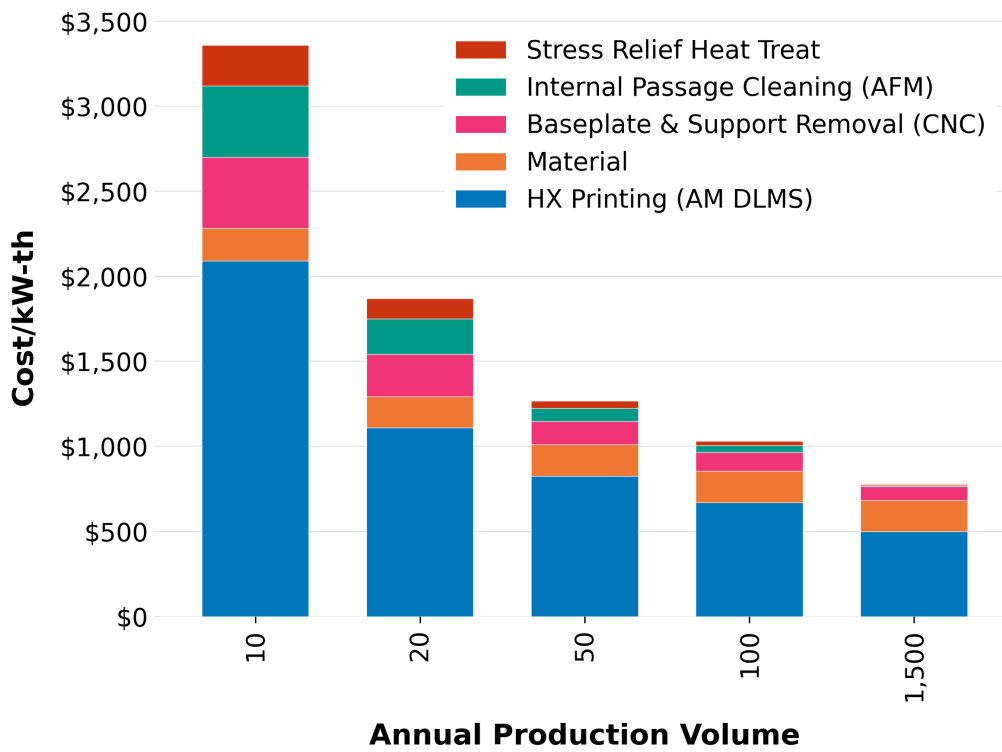
Figure 4: Breakdown of initial HX design cost by process step for various APV. AM is the most significant contributor to HX cost.
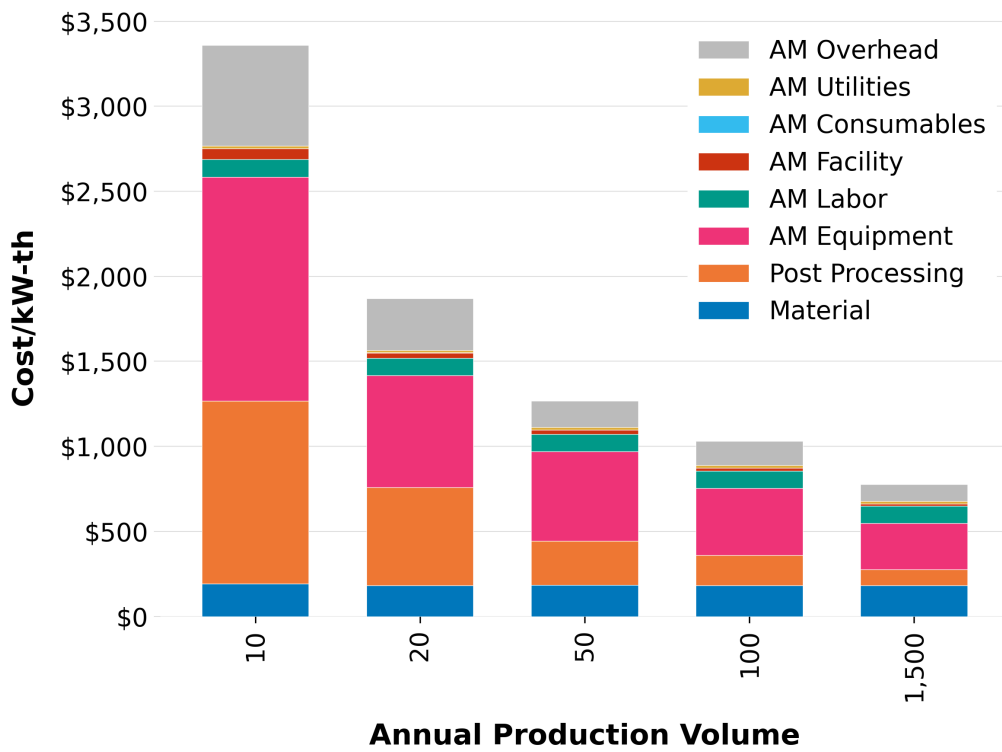
Figure 5: Breakdown of initial HX design cost with HX printing (AM) cost category for various APV. The most significant driver of AM cost is equipment cost.
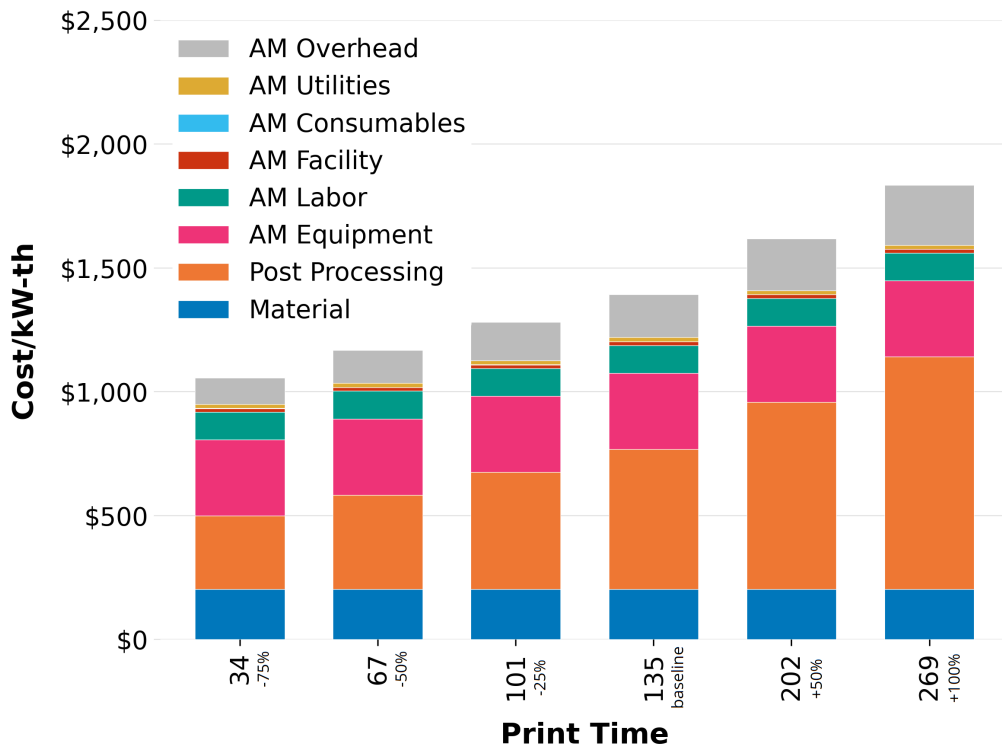
Figure 6: Breakdown of initial HX design cost for various print times (baseline print time is 135 hrs). Contributors to AM cost can be reduced by reducing print time. Costs shown assume APV 1,500 units.
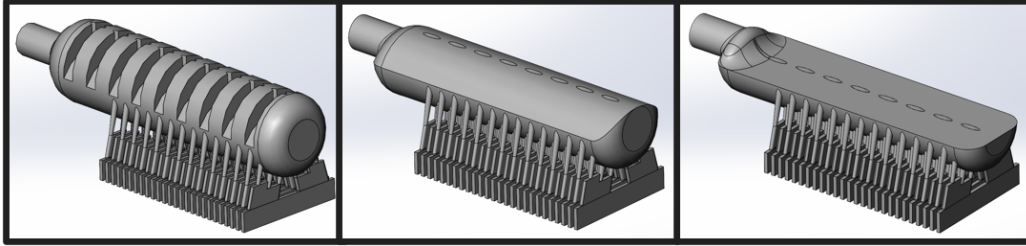
Figure 7: Internal design of header for: initial HX design (left), 25% volume reduction (center), and 50% volume reduction (right).

time by approximately 13%, and cost to \$600-720/kW-th. Reducing header volumes by 50% reduces material use by approximately 10%, print time by approximately 23%, and cost to \$540-640/kW-th. Based on this input from the cost model, we developed two alternative header designs, reducing header volume by 25 and 50%, as shown in Figure 7. Modeling of flow in pin array showed that reducing the header volume does not substantially impact flow distribution uniformity within the pin array.

Varying AM processing parameters to increase build rate allows us to reduce build time without changing HX thermal performance. However, adjusting the AM processing parameters impacts porosity defect generation in the HX. Figure 8 shows porosity measurements from test builds in Haynes 282 for multiple combinations of scan speed, laser power, and hatch spacing. Each porosity measurement is shown with the cost per kW-th for our HX design printed with corresponding AM processing parameters. From this data we see that two parameter sets minimize porosity (P 200W, v 760 mm/s, and P 250W, v 960 mm/s). This indicates that we can increase v from the baseline of 700 mm/s to 960 mm/s without increasing porosity (i.e. without degrading HX creep and fatigue life). Increasing v to 960 mm/s lowers the HX cost by approximately \$100/kW-th. Our current, conservative approach is to select process parameters that generate the lowest possible porosity. If parts with higher porosities maintain adequate mechanical properties, it may be possible to further increase printing speeds and therefore reduce cost further. Future work is needed to better understand the relationship between porosity and H282 material properties to determine if this is feasible.

Through the combination of the header re-design and increased laser scan speed of 960 mm/s, we can reduce the HX cost to \$530-610/kW-th. With the changes, the AM process step is still the largest contributor to total cost,
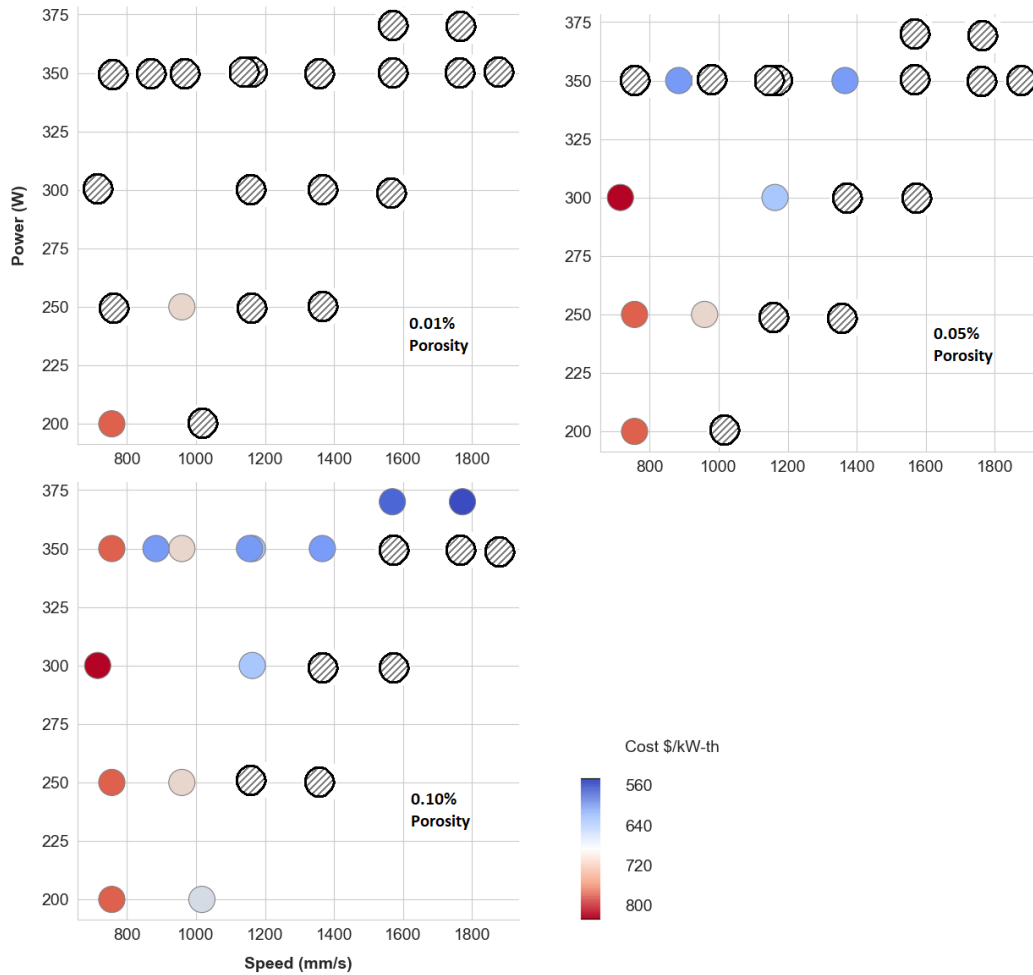
17

Figure 8: Each spot in these figures represents the cost/kW associated with producing HX in H282 with the given P and v parameter set. In each panel, test samples that exceeded the porosity threshold for that panel are blacked out. L for all parameter sets is 40 microns. H for all parameter sets is 110 microns except (884,350 - H 170), (1155,350 - H 130), and (1878,350 - H 80). Costs shown assume 1,500 unit APV.

accounting for approximately 60% of the cost.

To identify further avenues for cost reduction, we evaluated scenarios that can likely be achieved using currently commercially available technologies. This scenario analysis as well as the above-mentioned analysis of how cost responds to changes also constitutes a sensitivity analysis and a basic quantification of uncertainty. Analyzed scenarios include: improved powder removal methods to reduce fraction on trapped powder [46], leveraging production AM machine monitoring software to reduce required human monitoring [47], and using multi-laser machines to reduce print time [48]. Table 1 describes these scenarios. Figure 9 shows the impact of the header re-design, increase in laser scan speed, and the various AM process modification scenarios. Implementation of AM process modifications enabled by commercially available technologies could reduce HX cost further to approximately $400-450/kW-th.

A number of innovations in AM machines are currently under development to improve printing time and support production-scale AM. We evaluate scenarios that may be enabled by these future innovations. These scenarios include: increasing laser scan speed through higher power lasers, spot size control, or beam shaping [49, 50, 51], reducing setup/teardown time with automated setup and compartmentalized machines [49, 50], reducing heatup/cooldown time with dedicated cooling compartments [49], and improving part acceptance through lean/six-sigma process improvement [52]. Table 1 describes these scenarios. Figure 10 shows the impact on cost for these scenarios. If these scenarios are realized, they could lower HX cost further to $240-290/kW-th. In future work, we plan to perform expert elicitation to assess the likelihood that these future scenarios can be achieved in the medium-term future.
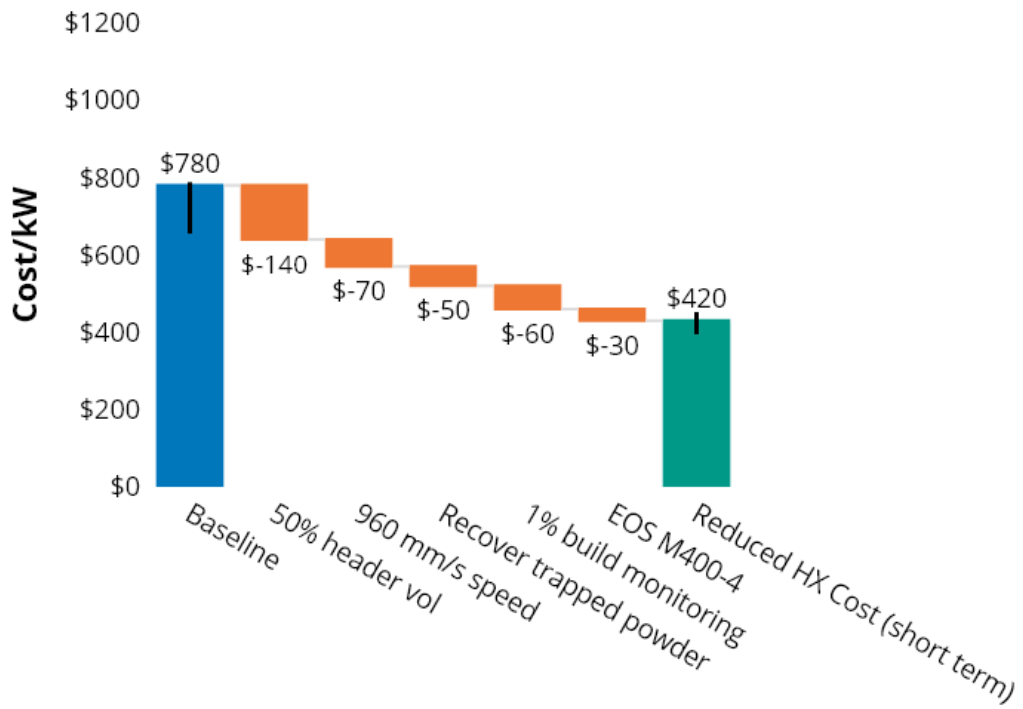
Figure 9: Cost reductions achieved through various measures that are likely feasible with current commercially available technology. Measures are arranged by likelihood to be immediately implementable with those that are most likely on the left. Table 4 contains a description of each scenario.
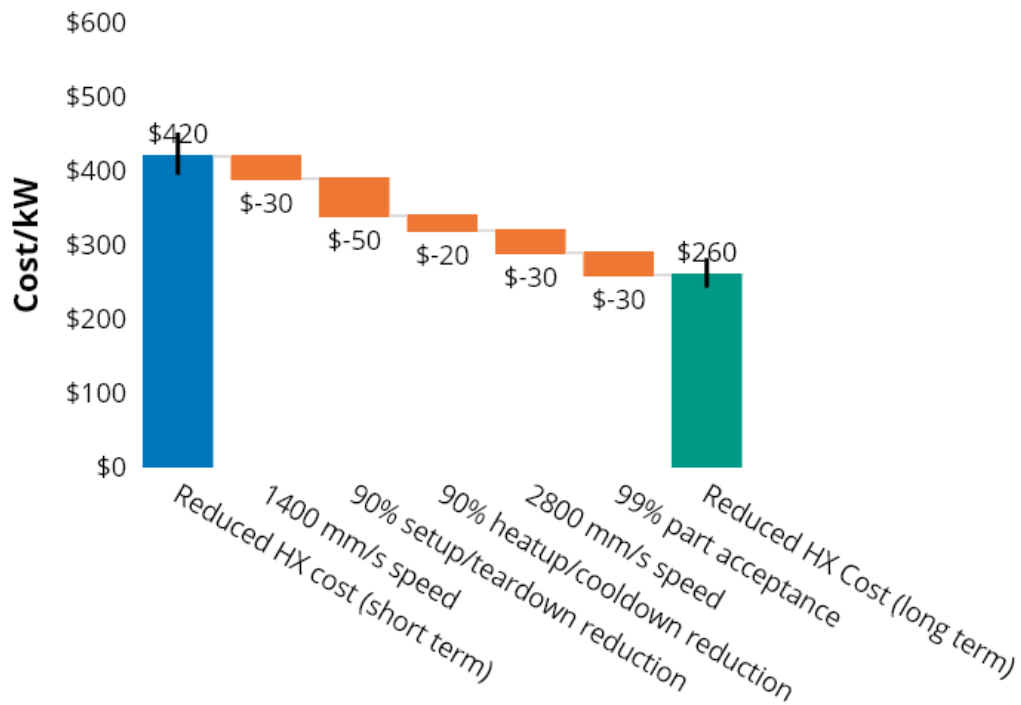
Figure 10: Cost reductions achieved through various measures that are may be feasible with medium-term technological innovation. Measures are arranged by likelihood to implementable in the longer term with those that are most likely on the left. Table 1 contains a description of each scenario.

Table 1: Scenarios modifying AM manufacturing process parameters. Short-term scenarios are likely possible with current commercially available technologies. Long-term scenarios may be possible in the future with innovations currently in development.

Scenario	Description	Variable Changed	Baseline Value	Scenario Value
Short-term Cost Reduction (enabled by current commercial technologies)				
Recover trapped powder	Recover and recycle unmelted powder trapped in plates*	trapped powder recycle fraction	0%	90%
1% Build monitoring	Reduce portion of the print time that must be monitored by a laborer**	cycle labor fraction	10%	1%
EOS M400-4	Switch to EOS M400-4 AM machine with 4 lasers and larger build area	raster time	t_r	$\frac{1}{4}t_r$
		build plate length	250 mm	400 mm
		machine price	$595k	$1.66m
Long-term Cost Reduction (enabled by techniques and technologies under development)				
1400 mm/s speed	Increase laser scan speed (from 960 mm/s speed in short-term reduction)	laser scan speed	960 mm/s	1400 mm/s
90% Setup/teardown reduction	Reduce time required to load and unload AM machine	setup/teardown time	4.5hr	0.5 hrs
90% Heatup/cooldown reduction	Reduce time required for AM machine pre-heating and cooldown	heatup/cooldown time	5hr	0.5hr
2800 mm/s speed	Increase laser scan speed (marginal cost reduction for increasing from 1400 to 2800 mm/s)	laser scan speed	1400 mm/s	2800 mm/s
99% Part acceptance	Reduce fraction of defective parts produced in printing HX	AM part acceptance rate	90%	99%

*Removal of trapped powder has been demonstrated in laboratory without additional equipment.

**Software license cost is negligible relative to overall part cost.

5. Conclusions

Developing a high efficiency, low cost MS-to-sCO$_2$ primary HX for use in CSP is critical to reducing CSP LCOE to be cost competitive with other sources such as fossil, nuclear, and wind. The baseline technology to manufacture high efficiency is microlamination by diffusion bonding, although it is unclear that microlamination can produce HXs with the properties required for CSP. AM has been demonstrated as a viable technique for fabricating high efficiency HX. We evaluate AM as an alternative to microlamination.

- If the HX is produced with lab-based process using a single-laser powder-bed fusion machine that is run continuously (24x7), and with very conservative process parameters, we find it would cost \$780/kW-th (\$650-790/kW-th) at APV 1,500 (the estimated number of units required for a 20MW CSP plant). 1500 units is far more than what is needed to achieve economies of scale.

- We integrate cost modeling into the design process and identify opportunities for sharp cost reductions. Reducing the volume of the HX headers by 50% and increasing laser scan speed from 700 mm/s to 960 mm/s, reducing the cost to \$530-610/kW-th.

- Incorporating additional AM process modifications possible with commercially available industrial scale AM technologies, cost is reduced to \$400-450/kW-th.

- We also evaluate AM machine innovations currently under development to improve speed and production-readiness of AM. If all evaluated improvements are are realized, they would cut HX cost to \$240-290/kW-th.

- It may be possible to further reduce cost through additional design changes to reduce HX volume or through AM processing parameter changes to increase build rate. However, evaluating these changes requires additional mechanical modeling and material performance data.

6. Acknowledgements

References

[1] DOE, DOE Pursues SunShot Initiative to Achieve Cost Competitive Solar Energy by 2020, `https://www.energy.gov/eere/solar/articles/doe-pursues-sunshot-initiative-achieve-cost-competitive-solar-energy-2020`, (Accessed on 09/24/2020) (2 2011).

[2] DOE, The SunShot Initiative's 2030 Goal: 3¢ per Kilowatt Hour for Solar Electricity, (Accessed on 09/24/2020) (01 2010).

[3] M. Mehos, C. Turchi, J. Jorgenson, P. Denholm, C. Ho, K. Armijo, On the Path to SunShot: Advancing Concentrating Solar Power Technology, Performance, and Dispatchability, SunShot (May) (2016) 1–66.

[4] DOE, Concentrating solar power, `https://www.energy.gov/sco2-power-cycles-renewable-energy-applications/concentrating-solar-power`, (Accessed on 12/20/2020).

[5] HEXCES, Hexces - technology, `http://www.hexces.com/technology`, (Accessed on 12/19/2020).

[6] J. Nestell, T. L. Sham, Asme code considerations for the compact heat exchanger, Oak Ridge National Laboratory, ORNL/TM-2015/401 (2015).

[7] M. Kapoor, K. Rozman, O. Dogan, J. Hawk, R. Saranam, P. McNeff, B. Paul, Diffusion bonding of h230 ni-superalloy for application in microchannel heat exchanger, Tech. rep., NETL (2016).

[8] I. Gibson, D. W. Rosen, B. Stucker, et al., Additive manufacturing technologies, Vol. 17, Springer, 2014.

[9] E. Rasouli, C. Davis, S. Subedi, C. Montgomery, C. Mande, W. C. E. Center, M. Stevens, V. Narayanan, A. Rollett, Design and performance characterization of an additively manufactured primary heat exchanger

for sco2 waste heat recovery cycles, in: Proceedings of the 6th International Symposium on Supercritical CO2 Power Cycles, Pittsburgh, PA, USA, 2018, pp. 27–29.

[10] D. Saltzman, M. Bichnevicius, S. Lynch, T. W. Simpson, E. W. Reutzel, C. Dickman, R. Martukanitz, Design and evaluation of an additively manufactured aircraft heat exchanger, Applied Thermal Engineering 138 (2018) 254–263.

[11] M. A. Arie, A. H. Shooshtari, M. M. Ohadi, Experimental characterization of an additively manufactured heat exchanger for dry cooling of power plants, Applied Thermal Engineering 129 (2018) 187–198.

[12] R. Tiwari, R. S. Andhare, A. Shooshtari, M. Ohadi, Development of an additive manufacturing-enabled compact manifold microchannel heat exchanger, Applied Thermal Engineering 147 (2019) 781–788.

[13] F. Field, R. Kirchain, R. Roth, Process cost modeling: Strategic engineering and economic evaluation of materials technologies, Jom 59 (10) (2007) 21.

[14] R. Kirchain, F. Field, Process-based cost modeling: understanding the economics of technical decisions, Encyclopedia of Materials Science and Engineering 2 (2001) 1718–1727.

[15] E. R. Fuchs, F. R. Field, R. Roth, R. E. Kirchain, Strategic materials selection in the automobile body: Economic opportunities for polymer composite design, Composites science and technology 68 (9) (2008) 1989–2002.

[16] R. E. Laureijs, J. B. Roca, S. P. Narra, C. Montgomery, J. L. Beuth, E. R. Fuchs, Metal additive manufacturing: cost competitive beyond low volumes, Journal of Manufacturing Science and Engineering 139 (8) (2017).

[17] H. Benson-Woodward, M. Koslowske, R. Kirchain, I. Bar-On, A performance based, multi-process cost model for solid oxide fuel cells, MRS Proceedings 756 (2002) FF4.10. doi:10.1557/PROC-756-FF4.10.

[18] A. Sakti, J. J. Michalek, E. R. Fuchs, J. F. Whitacre, A techno-economic analysis and optimization of li-ion batteries for light-duty passenger vehicle electrification, Journal of Power Sources 273 (2015) 966–980.

[19] J. B. Roca, P. Vaishnav, R. E. Laureijs, J. Mendonça, E. R. Fuchs, Technology cost drivers for a potential transition to decentralized manufacturing, Additive Manufacturing 28 (2019) 136–151.

[20] Z. Nie, S. Jung, L. B. Kara, K. S. Whitefoot, Optimization of part consolidation for minimum production costs and time using additive manufacturing, Journal of Mechanical Design 142 (7) (2020).

[21] E. Ulu, R. Huang, L. B. Kara, K. S. Whitefoot, Concurrent structure and process optimization for minimum cost metal additive manufacturing, Journal of Mechanical Design 141 (6) (2019).

[22] Q. Gao, J. Lizarazo-Adarme, B. K. Paul, K. R. Haapala, An economic and environmental assessment model for microchannel device manufacturing: part 1–methodology, Journal of cleaner production 120 (2016) 135–145.

[23] Q. Gao, J. Lizarazo-Adarme, B. K. Paul, K. R. Haapala, An economic and environmental assessment model for microchannel device manufacturing: part 2–application, Journal of Cleaner Production 120 (2016) 146–156.

[24] B. Paul, C. Song, K. Lee, B. M. Fronk, D. Sahoo, M. Shipley, Conceptual design of a manufacturing process for an automotive microchannel heat exchanger (2018).

[25] Haynes Internations, Haynes 282 Alloy (2020).

[26] EOS GmbH, Technical data - eos m 290, https://www.eos.info/en/additive-manufacturing/3d-printing-metal/eos-metal-systems/eos-m-290, (Accessed on 05/05/2020) (1 2019).

[27] T. M. Mower, M. J. Long, Mechanical behavior of additive manufactured, powder-bed laser-fused materials, Materials Science and Engineering: A 651 (2016) 198–213.

[28] A. B. Spierings, T. L. Starr, K. Wegener, Fatigue performance of additive manufactured metallic parts, Rapid prototyping journal (2013).

[29] H. Gong, K. Rafi, H. Gu, T. Starr, B. Stucker, Analysis of defect generation in ti–6al–4v parts made using powder bed fusion additive manufacturing processes, Additive Manufacturing 1 (2014) 87–98.

[30] R. W. Cunningham, Defect formation mechanisms in powder-bed metal additive manufacturing, Ph.D. thesis, Carnegie Mellon University (2018).

[31] M. Tang, P. C. Pistorius, J. L. Beuth, Prediction of lack-of-fusion porosity for powder bed fusion, Additive Manufacturing 14 (2017) 39–48.

[32] J. V. Gordon, S. P. Narra, R. W. Cunningham, H. Liu, H. Chen, R. M. Suter, J. L. Beuth, A. D. Rollett, Defect structure process maps for laser powder bed fusion additive manufacturing, Additive Manufacturing 36 (2020) 101552.

[33] NextManufacturing Carnegie Mellon University, Details and cost, https://engineering.cmu.edu/next/facilities/details-cost.html, (Accessed on 05/07/2020).

[34] Phillips Corporation Federal Division, Gs-03f-080ca phillips federal price list schedule 2020, https://www.gsaadvantage.gov/ref_text/GS03F080CA/0VGL91.3R6Y7S_GS-03F-080CA_GS03F080CAPHILLIPSFEDERAL07012020.PDF, (Accessed on 12/19/2020) (7 2020).

[35] DGI Supply, Doall dc-400cnc, https://www.dgisupply.com/product/CMIDC400CNC/;pgid=jkXWMVB7ulZSRphasW29_Dxt0000Mbr-8vXP;sid=Pu3DRFWI27XIRA7k -4gkROUkXEYNUshmvgJeqtVn, (Accessed on 12/22/2020).

[36] K. S. Fujita, Commercial discount rate estimation for efficiency standards analysis (2016).

[37] D. M. Dietrich, M. Kenworthy, E. A. Cudney, Additive Manufacturing Change Management: Best Practices, CRC Press, 2019.

[38] US Bureau of Labor Statistics, Engineering technicians, except drafters, all other, `https://www.bls.gov/oes/2017/may/oes173029.htm`, (Accessed on 11/11/2020) (05 2017).

[39] US Bureau of Labor Statistics, Employer costs for employee compensation for the regions – december 2019, `https://www.bls.gov/regions/southwest/news-release/ employercostsforemployee compensation_regions.htm`, (Accessed on 05/07/2020) (12 2019).

[40] ExtrudeHone, Product data sheet vector, `https://extrudehone.com/wp-content/uploads/2016/04/ 15001_EH_VECTOR_v06_Final.pdf`, (Accessed on 05/07/2020).

[41] Statista, Industrial rents per square foot by type u.s. 2018, `https://www.statista.com/statistics/626555/average-rent-per -square-foot-paid-for-industrial-space-usa-by-type/`, (Accessed on 05/05/2020) (11 2019).

[42] Global Industrial, Band saw blades, `https://www.globalindustrial.com/c/metalworking-tools/ metalworking-saw-blades/bandsaw-blades`, (Accessed on 12/19/2020).

[43] Global Industrial, Metal working fluids, `https://www.globalindustrial.com/c/metalworking-tools/ metal-fluids/metalworking-fluids-2`, (Accessed on 12/19/2020).

[44] B. Denkena, P. Helmecke, L. Hülsemeyer, Energy efficient machining with optimized coolant lubrication flow rates, Procedia CIRP 24 (2014) 25–31.

[45] US Energy Information Administration, Electric Power Monthly with data for February 2020, Tech. rep.

[46] Solukon, Solukon - metall, `https://www.solukon.de/en/metall/`, (Accessed on 12/23/2020).

[47] EOS GmBH, 3d printing software. industrial solutions for am production,

https://www.eos.info/en/additive-manufacturing/software-3d-printing, (Accessed on 12/23/2020).

[48] EOS GmbH, EOS M400-4, https://www.eos.info/en/additive-manufacturing/3d-printing-metal/eos-metal-systems/eos-m-400-4, (Accessed on 12/22/2020).

[49] SLM, SLM NXG XII 600 Detail Page, https://www.slm-pushing-the-limits.com/specs, (Accessed on 12/23/2020).

[50] TRUMPF, TruPrint Series 5000, https://www.trumpf.com/en_US/products/machines-systems/additive-production-systems/truprint-5000/, (Accessed on 12/23/2020).

[51] R. Shi, S. A. Khairallah, T. T. Roehling, T. W. Heo, J. T. McKeown, M. J. Matthews, Microstructural control in metal laser powder bed fusion additive manufacturing using laser beam shaping strategy, Acta Materialia 184 (2020) 284–305.

[52] H. Yang, P. Rao, T. Simpson, Y. Lu, P. Witherell, A. R. Nassar, E. Reutzel, S. Kumara, Six-sigma quality management of additive manufacturing, Proceedings of the IEEE (2020).